

## 11A.5 THE KINEMATIC AND THERMODYNAMIC EFFECTS OF VORTICIES WITHIN A DRYLINE

Michael S. Buban<sup>1,\*</sup>, Conrad L. Ziegler<sup>2</sup>, and Erik N. Rasmussen<sup>1</sup>

<sup>1</sup>Cooperative Institute for Mesoscale Meteorological Studies (CIMMS), University of Oklahoma, Norman OK

<sup>2</sup>NOAA/National Severe Storms Laboratory, Norman OK

### I. INTRODUCTION

During the late afternoon and evening of 22 May 2002, high resolution data from numerous platforms were collected over the north-east Texas and eastern Oklahoma panhandles over which a sharpening dryline had become established. This data was obtained as part of the International H<sub>2</sub>O Project (IHOP). Using this data, we set out to document the presence of small-scale vorticies along the dryline and determine their kinematic and thermodynamic properties. Additionally, in this study we will test two hypotheses: 1) that these vorticies are associated with local maxima in vertical velocity, specific humidity, virtual potential temperature, and the presence of cumulus, and 2) that deep cumulus development requires the mesoscale updraft's parcels to achieve their Lifted Condensation Level (LCL) and Level of Free Convection (LFC) prior to detraining from the updraft. This latter hypothesis is expressed via dimensionless relations among the horizontal and vertical length and velocity scales, including the LCL and LFC as "vertical moisture" length scales. In this paper we will discuss the data analysis techniques and present some multiple-Doppler radar and mobile mesonet analyses.

### 2. DATA AND ANALYSIS

By early afternoon, a weak dewpoint gradient had developed over the Intensive Observing Region (IOR) and, as the afternoon progressed, had tightened to form a pronounced dryline. The dryline was being sampled by 7 mobile mesonets which were taking in situ measurements of temperature, relative humidity, pressure, and wind velocity. The mesonets performed transects perpendicular to the dryline and collected data at one second intervals. Also collecting data were 4 mobile Doppler radars: SMART radar (SR-1), DOW-2, DOW-3, and XPOL. The radars were set up in a diamond pattern, each taking 140° sector scans

centered on the dryline. This configuration was employed in order to maximize baseline angles and allow for optimal multiple Doppler wind synthesis. Between approximately 2230 through 0100 (all times are Universal Time) between 3 and 4 of these radars were taking continuous data of the dryline and surrounding environment. The radars were time synched and volume scans were collected at 3 minute intervals with an average radar beam width  $\sim 1.0^\circ$  and gate length  $\sim 100$  m, making for a high spatial and temporal resolution dataset. Also participating in the data collection were a mobile CLASS and 2 mobile GLASS sounding systems, 3 research aircraft, the UAH profiling system (MIPS), a mobile radiometer (DRI), and a Scanning Raman Lidar (SRL).

During radar post-analysis, the data were edited to correct orientation, remove ground targets and weak signals, and dealias velocities. The data were then individually interpolated, using a Barnes objective analysis scheme, to regular Cartesian grid using a modified version of the NCAR Reorder software. The choice of Barnes smoothing parameter yielded a theoretical response of  $\sim 50\%$  at a wavelength of 0.83 km and  $\sim 5\%$  at a wavelength of 0.4 km. The grid spacing was set to 500 m in the horizontal and 250 m in the vertical with dimensions of 50 x 50 x 2 km, corresponding to 101 x 101 x 9 grid points respectively. The grid spacing and Barnes weighting function were chosen to capture the small scale features of the flow while minimizing unwanted noise. The objectively analyzed radial velocities were then combined, using the NCAR Reorder software, to solve an overdetermined set of linear equations for the velocities on horizontal planes. Vertical velocities were finally obtained by integrating the mass continuity equation with a boundary condition of  $w = 0$  at the ground level.

Data collected from the mobile mesonets were used to obtain thermodynamic characteristics of the near surface dryline environment. Since the mesonet data were collected along one-dimensional transects (i.e. along east-west roads), the horizontal resolution of the data was limited by the vehicle spacing. To fill in data gaps, a time-to-space conversion technique was developed to extract instantaneous two-dimensional spatial fields from one-dimensional data in space and

\*Corresponding author address: Michael S. Buban, CIMMS/NSSL, 1313 Halley Circle, Norman, OK 73069

time. In this procedure, the data were initially temporally smoothed using a four-pass application of a triangular weighting function, varying linearly from 0 at  $\pm 12$  s to 1 at the observation time (e.g. Ziegler and Rasmussen 1998). Trajectories from multiple-Doppler radar derived velocities were then computed from each observation location using an iterative second order predictor-corrector procedure. Finally, observations were advected along computed trajectories either forward or backward in time to the reference analysis time. An example of observations advected using this technique is shown in fig. 2.

### 3. RESULTS

Through the late afternoon the dryline was oriented almost due north-south and remained quasi-stationary within the IOR before retreating to the west during the early evening. The dryline was characterized by a strong moisture gradient residing in a confluence zone and a region of enhanced reflectivity and vertical velocity. West of this feature, a secondary post-dryline boundary was located as a weaker moisture

gradient, zone of enhanced reflectivity, confluence, and vertical velocity (figs. 1-2). In addition to the associated moisture gradient, a gradient of virtual potential temperature ( $\theta_v$ ) was present across the dryline (fig. 2), and  $\theta_v$  varied as much as 2 K over 3 km, a similar magnitude to that found by Atkins et. al, (1998). The above boundaries also featured isolated regions of enhanced vertical vorticity and vertical velocity. These vorticies were  $\sim 2-4$  km in width with average vertical vorticity values  $\sim 3-9 \times 10^{-3} \text{ s}^{-1}$  and appeared to be associated with the isolated regions of enhanced vertical velocities (fig. 3). Mobile mesonet observations of mixing ratio suggest that these vorticies act to transport water vapor horizontally. It is hypothesized that interaction of the vorticies with the dryline may act to increase vertical motion, deepen the moist layer, and increase the probability of convection initiation.

The environment west of the dryline was very warm and dry with temperatures in the lower 30's C and dewpoints near 0° C. This environment was also characterized by convection organized into horizontal convective rolls (HCRs) with horizontal

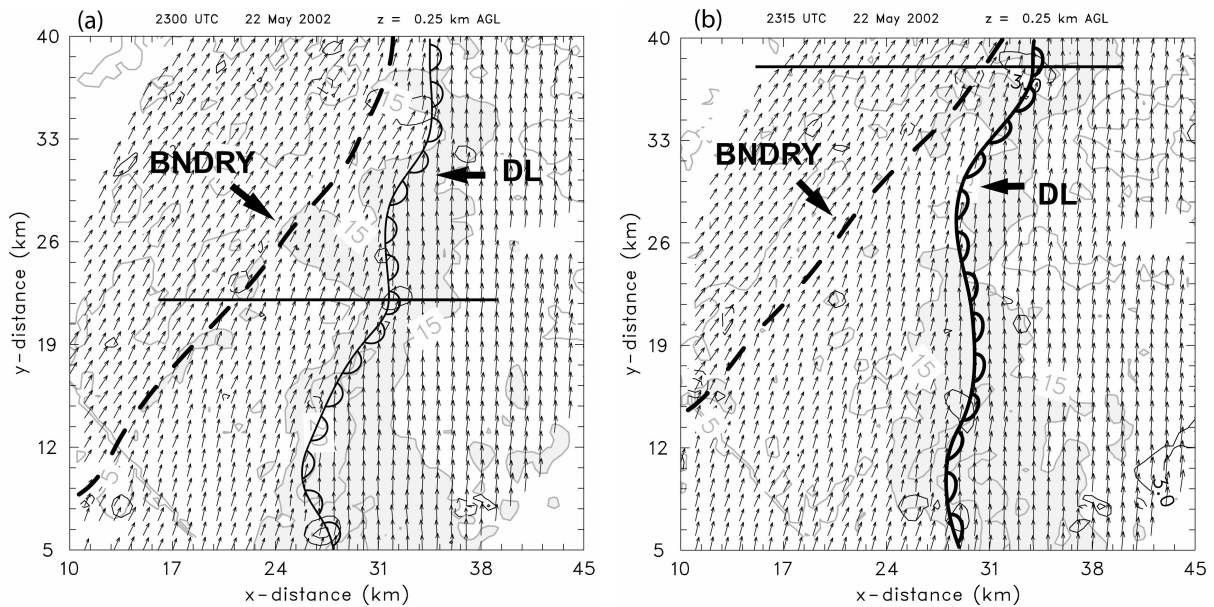


Figure 1 Horizontal wind vectors plotted at every other grid point ( $1 \text{ km} = 20 \text{ m s}^{-1}$ ), SR-1 derived reflectivity (contours every 5 dBZ starting at 10 dBZ with values above 15 dBZ shaded), and vertical vorticity ( $\text{s}^{-1} \times 10^{-3}$ ) (contours every  $3 \times 10^{-3}$  starting at  $3 \times 10^{-3}$ ) at  $z = .25 \text{ km}$  from quadruple-Doppler analysis. (a) 2300; (b) 2315. Positions of the dryline and post-dryline boundary are also shown. Heavy horizontal lines indicate locations of cross-sections in fig. 3.

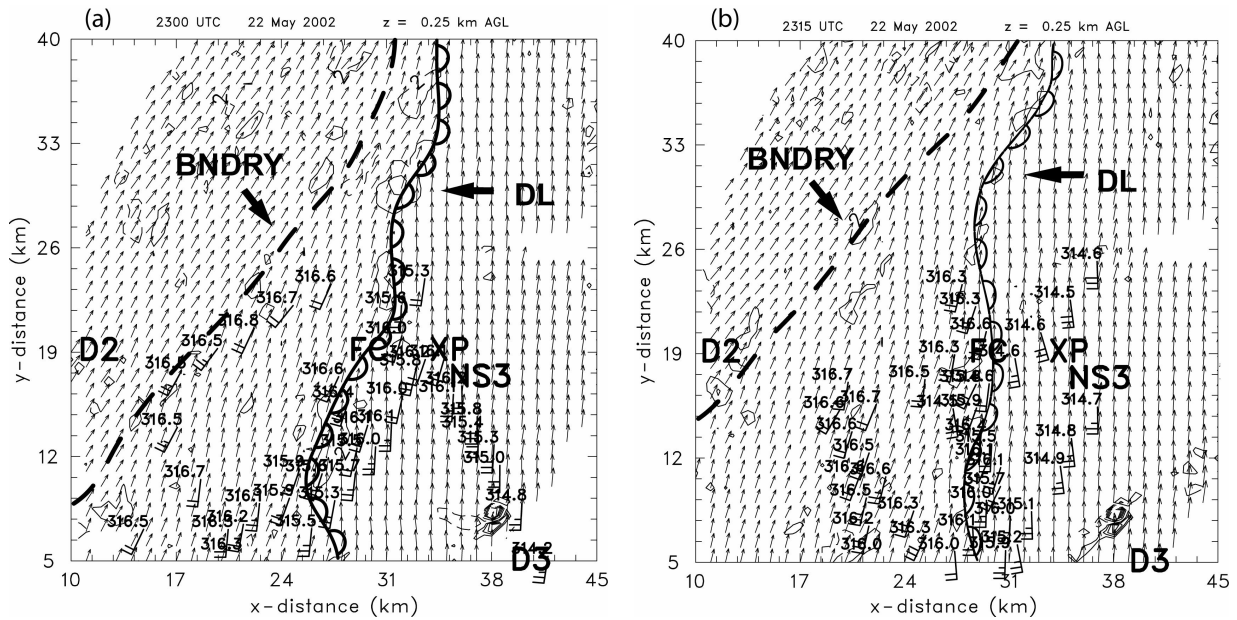


Figure 2 (a) Quadruple-Doppler analysis of horizontal wind vectors plotted at every other grid point ( $1 \text{ km} = 20 \text{ m s}^{-1}$ ), vertical velocity (contours every  $2 \text{ m s}^{-1}$  starting at  $2 \text{ m s}^{-1}$ ) at  $z = .25 \text{ km}$ , and a  $\pm 6$  minute window of mobile mesonet derived virtual potential temperature ( $\theta_v$ ) (K) and winds (full barb = 10 kts, half barb = 5 kts) plotted using time- to-space conversion and 90 s spacing between observations for each mesonet. (b) Same as (a) but for 2315. Locations of the field coordinator vehicle (FC), DOWs 2-3 (D2, D3), X-Pol (XP), and NSSL-3 (NS3) and positions of the dryline and post-dryline boundary are also shown.

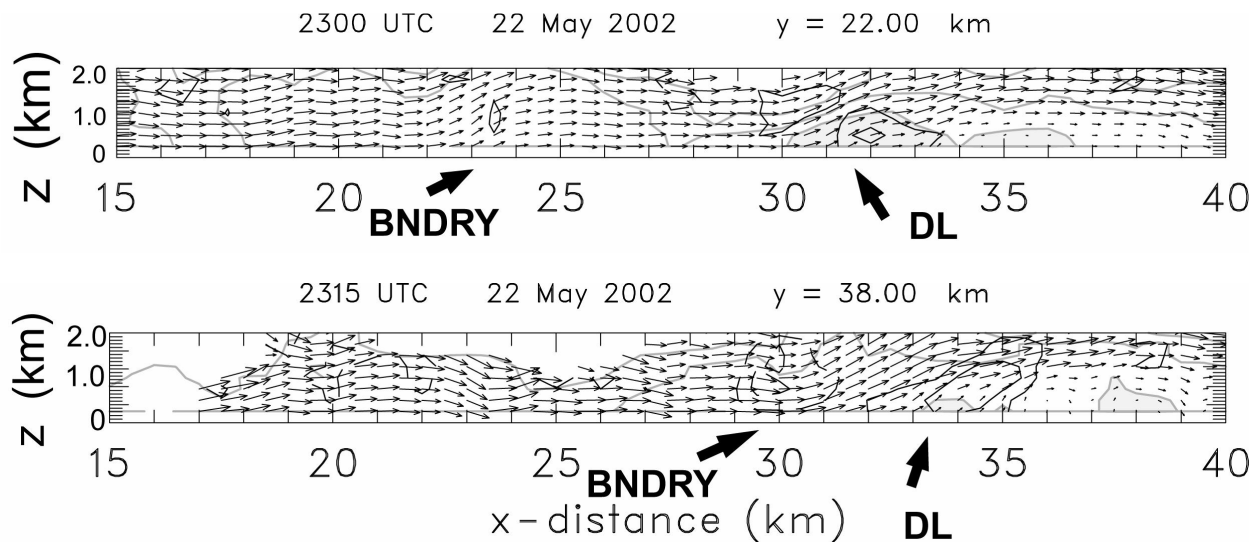


Figure 3 Wind vectors ( $1 \text{ km} = 15 \text{ m s}^{-1}$ ), SR-1 derived reflectivity (contours every 5 dBZ starting at 5 dBZ with values above 15 dBZ shaded), and vertical vorticity ( $\text{s}^{-1} \times 10^{-3}$ ) (contours every  $3 \times 10^{-3} \text{ s}^{-1}$  starting at  $3 \times 10^{-3} \text{ s}^{-1}$ ). (a) cross-section at 2300 at  $y = 22 \text{ km}$  as indicated in Fig. 1a; (b) same as in (a) but for 2315 at  $y = 38 \text{ km}$  as indicated in fig. 1b. Locations of the dryline and post-dryline boundary are indicated.

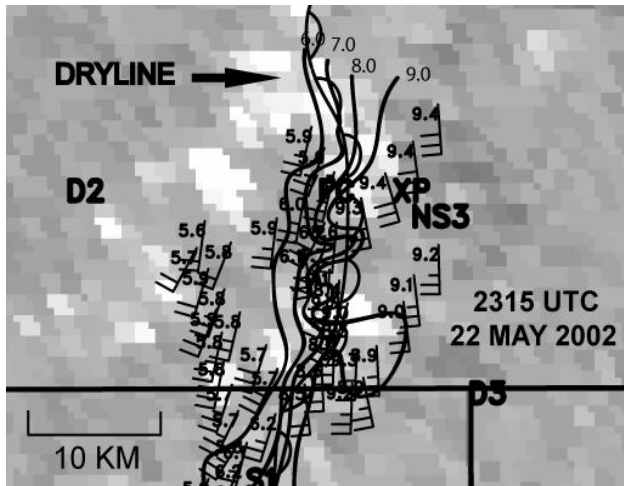
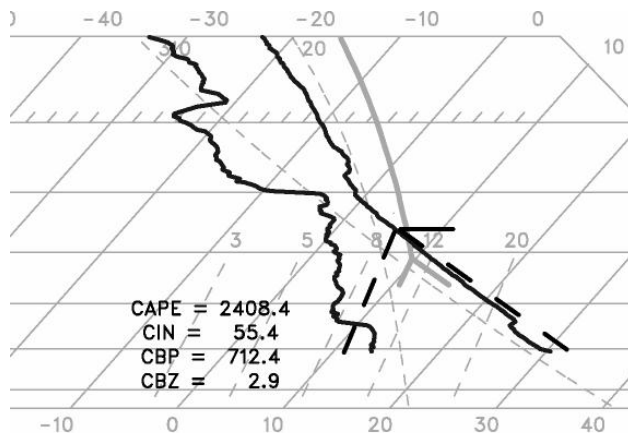


Figure 4. Mobile mesonet observations of mixing ratio (g/kg) and winds (kts) plotted using a time-to-space conversion technique and superimposed on a 1 km resolution GOES-8 visible satellite image at 2315. Contours are isolines of mixing ratio at 1g/kg intervals



NSSL M-CLASS 22 May 2002 2313 UTC

Figure 5. M-CLASS sounding taken east of the dryline at the location marked NS3 on fig. 4 at 2313. The light gray curve denotes a lifted parcel path and CAPE, CIN, cloud bases pressure (CBP), and cloud base height (CBZ) are indicated. The thick dashed curves show the properties of a lifted surface parcel using average mobile mesonet observations along the eastern edge of the dryline with the thick horizontal line marking the LCL.

spacing ~ 2-4 km. Eastward, along the eastern edge of the dryline the boundary layer was slightly cooler and

moister. Even so, along the moist side of the dryline, relative humidities were only around 25-30% and LCL heights were near 3 km as seen in fig. 5. Although deep convection did not develop in the IOR, shallow, high based cumulus were present along the dryline during the most of the afternoon into the evening. (fig 4).

#### 4. DISCUSSION

We are continuing our analysis of the radar and mobile mesonet data and are in the process of re-navigating available satellite data to the radar grid. Using a similar time-to-space conversion technique we are working on an objective analysis scheme to map the in situ mobile mesonet observations to the same grid. In addition we are analyzing other data sources such as the M-CLASS and M-GLASS soundings and in situ aircraft data. Using this data in concert with the gridded analyses we will test the two convective initiation hypotheses. These tests will take the form of correlations among parameters and 2 x 2 contingency table of predicted vs. observed cumulus. These results and further analyses will be presented at the conference.

#### 5. ACKNOWLEDGMENTS

The authors would like to thank Bob Rabin for his help with the re-navigating and display of the GOES-8 satellite data. We acknowledge the assistance of Dick Oye and Jay Miller with the NCAR Solo, Reorder, and Cedric software packages. Partial funding for this research was provided by National Science Foundation (NSF) grant ATM-013016.

#### 6. REFERENCES

- Atkins, N. T., R.M. Wakimoto, and C. L. Ziegler, 1998: Observations of the finescale structure of the dryline during VORTEX 95, *Mon. Wea. Rev.*, **126**, 525-549.
- Ziegler, C. L., and E. N. Rasmussen, 1998: The initiation of moist convection at the dryline: forecasting issues from a case study perspective, *Wea. Forecasting*, **13**, 1106-1131.